

# Rab11-FIP3 Is Critical for the Structural Integrity of the Endosomal Recycling Compartment

Conor P. Horgan<sup>1</sup>, Arkadiusz Oleksy<sup>1</sup>,  
Alexander V. Zhdanov<sup>1</sup>, Patrick Y. Lall<sup>2</sup>,  
Ian J. White<sup>3</sup>, Amir R. Khan<sup>4</sup>, Clare E. Futter<sup>3</sup>,  
John G. McCaffrey<sup>2</sup> and Mary W. McCaffrey<sup>1,\*</sup>

<sup>1</sup>Molecular Cell Biology Laboratory, Department of Biochemistry, Biosciences Institute, University College Cork, Cork, Ireland

<sup>2</sup>Department of Chemistry, National University of Ireland–Maynooth, Maynooth, Co. Kildare, Ireland

<sup>3</sup>Division of Cell Biology, Institute of Ophthalmology, University College London, London EC1V 9EL, UK

<sup>4</sup>School of Biochemistry and Immunology, Trinity College, Dublin 2, Ireland

\*Corresponding author: Mary W. McCaffrey, m.mccaffrey@ucc.ie

**Rab11-FIP3 is an endosomal recycling compartment (ERC) protein that is implicated in the process of membrane delivery from the ERC to sites of membrane insertion during cell division. Here we report that Rab11-FIP3 is critical for the structural integrity of the ERC during interphase. We demonstrate that knockdown of Rab11-FIP3 and expression of a mutant of Rab11-FIP3 that is Rab11-binding deficient cause loss of all ERC-marker protein staining from the pericentrosomal region of A431 cells. Furthermore, we find that fluorophore-labelled transferrin cannot access the pericentrosomal region of cells in which Rab11-FIP3 function has been perturbed. We find that this Rab11-FIP3 function appears to be specific because expression of the equivalent Rab11-binding deficient mutant of Rab-coupling protein does not perturb ERC morphology. In addition, we find that other organelles such as sorting and late endosomes are unaffected by loss of Rab11-FIP3 function. Finally, we demonstrate the presence of an extensive coiled-coil region between residues 463 and 692 of Rab11-FIP3, which exists as a dimer in solution and is critical to support its function on the ERC. Together, these data indicate that Rab11-FIP3 is necessary for the structural integrity of the pericentrosomal ERC.**

**Key words:** coiled coil, endosomal recycling compartment, Nuf, Rab11, Rab11-FIP3

**Received 24 August 2006, revised and accepted for publication 18 January 2007**

Compartmentalization in eukaryotic cells necessitates highly dynamic transport of proteins and lipids between distinct membrane-bound organelles. Organelles of the endocytic and secretory pathways exist as long-lived structures; therefore, dynamic exchange of material between these compartments requires the formation of

transport intermediates in the form of vesicles or tubules. The endosomal recycling compartment (ERC) is one such organelle that functions in the recycling of endocytosed material back to the cell surface (1).

The ERC is a mildly acidic (pH 6.4–6.5) compartment with tubulovesicular morphology that, in many cell types, is condensed around the microtubule organizing centre/centrosome [for a recent review see Maxfield and McGraw (1)]. The ERC undergoes intense trafficking activity connecting the endocytic and exocytic pathways; however, the majority of molecules in the ERC are returned to the plasma membrane (PM) (1). The Rab11 GTPase subfamily members (Rab11a, Rab11b and Rab25) are enriched on the ERC and are known to control traffic through this subpopulation of endosomes (2–4). Rab11 functionality is achieved by interaction with a complement of effector molecules that bind preferentially to GTP-bound Rab11. Recently, a Rab11 family of interacting proteins, the Rab11-FIPs, was identified and found to be enriched on the Rab11-positive ERC (5–8). Class I Rab11-FIPs [Rab-coupling protein (RCP), Rip11 and Rab11-FIP2] have been implicated in receptor recycling processes (7,9–11). Conversely, there is no evidence that the class II Rab11-FIPs (Rab11-FIP3 and Rab11-FIP4) play direct roles in receptor recycling to the cell surface. In addition to their ability to bind Rab11 subfamily members, class II Rab11-FIPs (also called arfophilins) are capable of interacting with members of the ADP ribosylation factor (ARF) GTPase family (12,13). Class II Rab11-FIPs localize to the pericentrosomal ERC during interphase and have been implicated in the processes of delivery, targeting and/or fusion of the ERC with the cleavage furrow/midbody during cell division (5,8,14,15). However, to date, the interphase function of the class II Rab11-FIPs has remained elusive.

Work in developmental models has identified Nuclear fallout (Nuf), the *Drosophila melanogaster* homologue of the class II Rab11-FIPs, as an important component of the ERC. Nuf and Rab11 were found to be mutually required for their intracellular localizations to the ERC (16). Additionally, it was found that following asymmetric cell division in sensory organ precursor (SOP) cells in which only one daughter cell receives Nuf, the cell devoid of Nuf fails to produce a pericentrosomal ERC (17).

In the present study, we demonstrate that Rab11-FIP3 is critical for the structural integrity of the ERC during interphase in A431 cells. We find that suppression of Rab11-FIP3 expression results in loss of the pericentrosomal ERC, and that this Rab11-FIP3 function occurs in an Rab11-dependent fashion. Finally, we show that Rab11-FIP3

contains an extensive coiled-coil region which dimerizes in solution, and is critical for its ERC-related function.

## Results

### ***Rab11-FIP3 expression is essential for ERC structural integrity***

Evidence from *D. melanogaster* identifies Nuf as an integral component of recycling endosomes that is required for correct intracellular localization of Rab11 (16,17). We have previously demonstrated that exogenous expression of Rab11-FIP3 and Rab11-FIP4 profoundly alters the morphology of the ERC, condensing it into the pericentrosomal region of the cell (5,8). A similar phenotype is observed when Nuf is overexpressed in mammalian cells (12). These data suggest that class II Rab11-FIPs/Nuf could be important for the structural integrity of the ERC.

To establish if indeed Rab11-FIP3 is critical for the structural integrity of the ERC, we investigated by RNA interference (RNAi) the effects inhibition of Rab11-FIP3 expression has on the morphology of this compartment. Significant reduction in Rab11-FIP3 levels (knockdown) was achieved 72 h post-transfection of A431 cells with 30 nM Rab11-FIP3 siRNA, as assessed by immunofluorescence (Figure 1A) and Western blot (Figure 1B, upper panel). No such effect was observed on Rab11-FIP3 expression levels in control (non-targeting) siRNA-transfected samples when compared with mock (no siRNA) transfected samples (data not shown). Notably, we did find that knockdown of Rab11-FIP3 resulted in cell death, as a proportion of cells appear necrotic/apoptotic having detached from the plate in Rab11-FIP3 knockdown, but not control transfected, samples. We estimate the extent of this cell death to be approximately 20–25% (data not shown). Interestingly, we found that upon immunolabelling Rab11-FIP3 knockdown samples, all ERC-marker proteins tested were absent from the pericentrosomal region of A431 cells, while control siRNA transfection had no effect (Figure 2). For RCP, a class I Rab11-FIP reported to extensively label the ERC (7), we found that in control transfected cells, approximately 95% of cells display strong staining in the pericentrosomal region of the cell (Figure 2A,B). However, in Rab11-FIP3 knockdown samples, we found that RCP displayed reduced pericentrosomal staining, with only approximately 40% of cells retaining the RCP in this region of the cell (Figure 2A,B). Additionally, it is notable that in knockdown samples, cells had slightly elongated morphology and RCP was concentrated at the periphery (Figure 2A, arrow). Rab11a, the best known ERC-marker protein (18,19), and a key molecule with which Rab11-FIP3 interacts (6), was found at the pericentrosomal region of the cell in approximately 45% of Rab11-FIP3 siRNA-treated cells (Figure 2A,B). Conversely, in control samples, 95% of cells display strong Rab11a pericentrosomal staining (Figure 2A,B). On examination of the localization of Rab11-FIP4, the other class II Rab11-FIP,

we found that this protein was also dramatically lost from the pericentrosomal region of the cell on Rab11-FIP3 knockdown (Figure 2A,B).

To determine if knockdown of Rab11-FIP3 actually disrupted the ERC or simply mislocalized Rab11, along with the proteins with which Rab11 specifically interacts, we examined the localization of further ERC-marker proteins in cells in which Rab11-FIP3 had been depleted. RME-1 is one such protein that localizes to the Rab11-FIP3-positive ERC [Figure S1 (20,21)]. We found that, in control samples, approximately 45% of cells display pericentrosomal, in addition to peripheral, staining for RME-1, but on knockdown of Rab11-FIP3 only approximately 8% of cells have retained pericentrosomal staining for this protein (Figure 2A,B).

We next examined the localization of the transferrin receptor (TfnR) in cells depleted of Rab11-FIP3. The TfnR is a classical receptor recycling marker protein that localizes primarily to sorting endosomes and the ERC at steady state (1). Like all the other ERC-marker proteins tested, we found that pericentrosomal staining of the TfnR was reduced on knockdown of Rab11-FIP3 (Figure 2A,B). Next, because the TfnR and its ligand transferrin (Tfn) traffic through the ERC (1), we performed a Tfn uptake assay to determine if fluorophore-labelled Tfn was capable of accessing the pericentrosomal region of cells depleted of Rab11-FIP3. We found that following 45 min of continuous uptake of Alexa 594-labelled Tfn in Rab11-FIP3 siRNA-treated samples, the Tfn failed to reach the pericentrosomal region of the cell (Figure 2A,B). In control samples, approximately 80% of cells display pericentrosomal labelling for Tfn, but in Rab11-FIP3-depleted samples, only approximately 28% of cells have pericentrosomal Tfn (Figure 2A,B).

To determine if the effects we observed on Rab11-FIP3 knockdown were limited to a subpopulation of endosomes, namely the ERC, we immunolabelled control and Rab11-FIP3 knockdown samples for early endosomal antigen (EEA1) and lysobisphosphatidic acid (LBPA), two well-characterized markers of early/sorting and late endosomes, respectively (22,23). No discernible perturbation of the localization of either of these endosomal markers was observed on Rab11-FIP3 knockdown (Figure 3). In addition, as the Rab11-FIP3-positive ERC is a pericentrosomal compartment (5), we determined if Rab11-FIP3 knockdown would perturb the centrosome. Immunolabelling control and Rab11-FIP3 knockdown samples with the centrosomal marker  $\gamma$ -tubulin (24) revealed that this structure is unaffected by inhibition of Rab11-FIP3 expression (Figure 3).

Because our light microscopy analyses indicate a loss of the ERC upon Rab11-FIP3 knockdown, we determined if similar effects were evident in Rab11-FIP3 knockdown samples analysed by electron microscopy. Cells were incubated for 45 min in the presence of Tfn conjugated to horseradish peroxidase (HRP) (Tfn-HRP). The Tfn-HRP, and thus the ERC, was then visualized following incubation of the cells

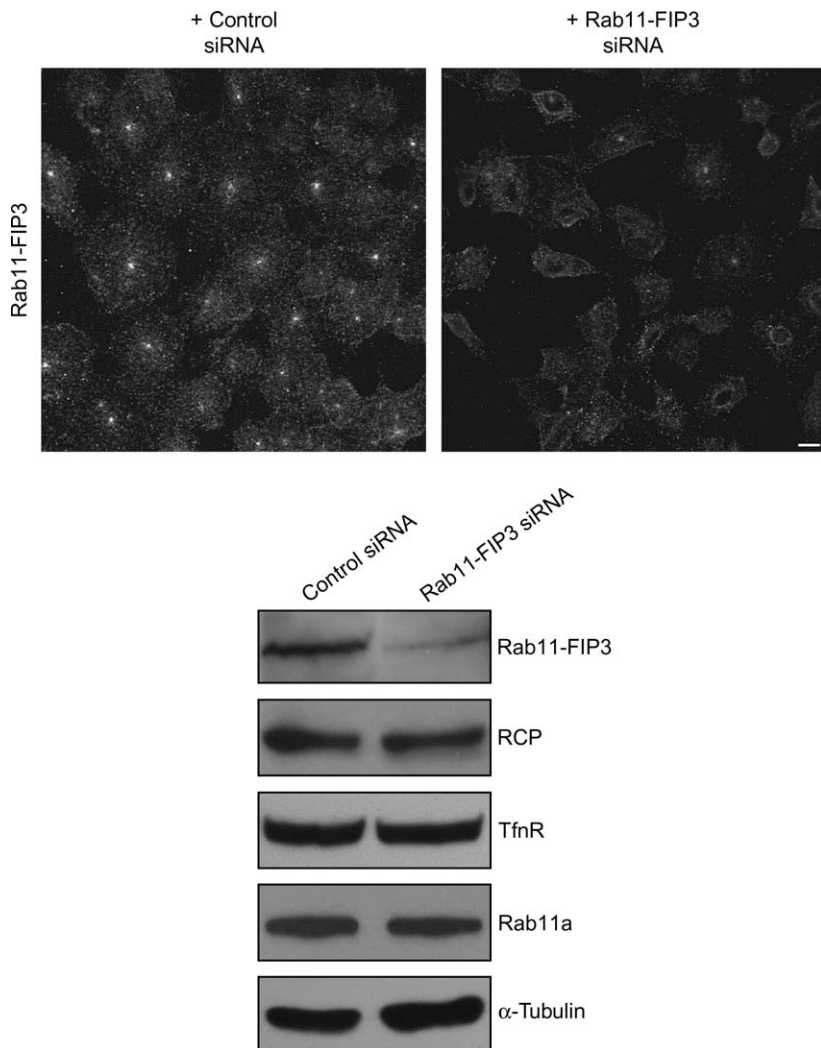


**Figure 1: Rab11-FIP3 knockdown does not affect ERC-marker protein levels.**

A) A431 cells were treated with control or Rab11-FIP3 siRNA. Seventy-two hours post-transfection the cells were processed for immunofluorescence and immunostained with an antibody to Rab11-FIP3. Scale bar represents 10  $\mu\text{m}$ . B) One hundred micrograms (150  $\mu\text{g}$  for Rab11-FIP3 blot) of total cellular lysate from control or Rab11-FIP3 siRNA-treated A431 cells was analysed by SDS-PAGE and immunoblotted with antibodies to Rab11-FIP3, RCP, TfnR, Rab11a or  $\alpha$ -tubulin. These data are typical of at least three separate experiments.

with diaminobenzidine (DAB) and hydrogen peroxide to form an electron-dense reaction product. The surrounding area in all sections showing a centriole was examined, and importantly those corresponding areas in sections both directly above and below the centrioles. The presence of structurally and functionally normal sorting and late endosomes (data not shown), and intact centrioles in both control and Rab11-FIP3 knockdown samples, confirmed our earlier findings that these structures remain unaffected by Rab11-FIP3 knockdown. Control cells showed a concentration of Tfn-HRP-positive small vesicles and tubules directly around the centrioles, indicative of the ERC. In contrast, the area immediately surrounding the centrioles in Rab11-FIP3 knockdown cells showed little, if any, staining for Tfn-HRP, and moreover, frequently showed few vesicular/tubular elements at all (Figure 4). This would suggest that the ERC itself has been largely lost rather than that the Tfn-HRP failed to traffic through an intact compartment.

Knockdown of RCP has previously been shown to result in a decrease in the total cellular levels of the TfnR (25).

As we had found that knockdown of Rab11-FIP3 perturbs ERC-marker protein localization (Figures 2 and 4), we determined if Rab11-FIP3 knockdown affects the expression levels of ERC-marker proteins such as RCP, TfnR and Rab11a. Equal amounts of A431 total cellular lysate from control and Rab11-FIP3 knockdown samples were analysed by Western blot as revealed by the  $\alpha$ -tubulin (Figure 1B, bottom panel). In contrast to the effect observed upon RCP knockdown (25), the expression levels of all ERC-marker proteins examined were unaffected by knockdown of Rab11-FIP3 (Figure 1B, RCP, TfnR and Rab11a blots).

Together, these data indicate that inhibition of Rab11-FIP3 expression results in loss of the pericentrosomal ERC structure while other endosome populations and the centrosome appear unaffected.

#### ***Rab11-FIP3 function at the ERC is Rab11 mediated***

Because Rab11-FIP3 is thought to be recruited to the ERC by Rab11 (14), and evidence from *D. melanogaster*

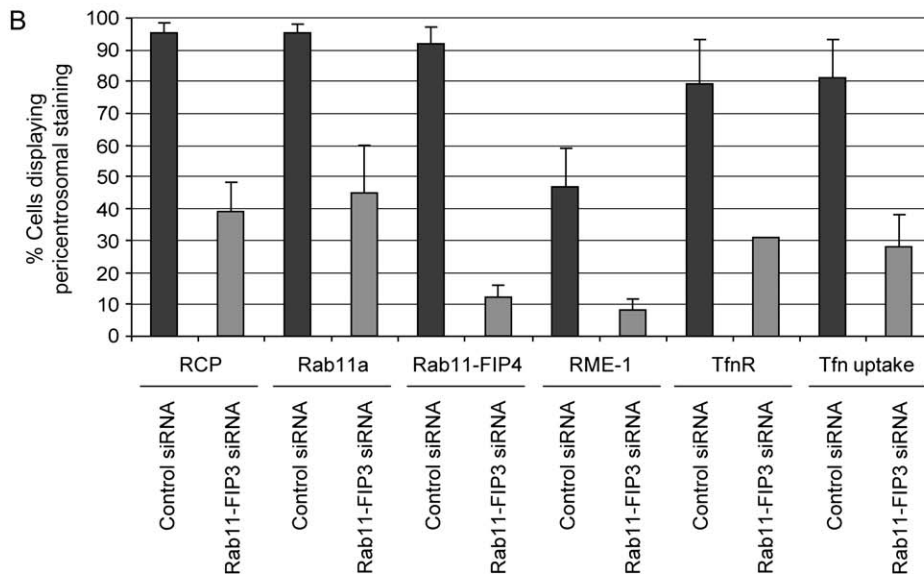
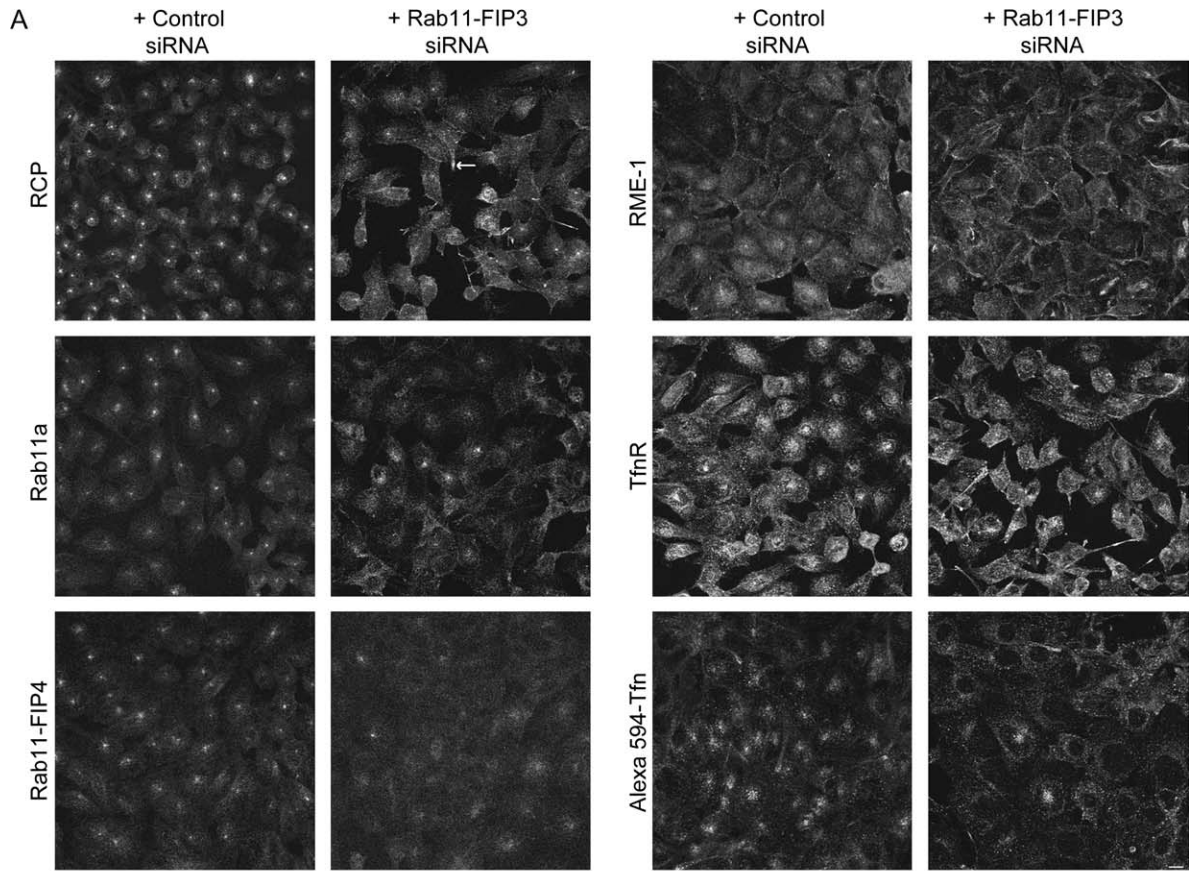


**Figure 2: Rab11-FIP3 knockdown causes loss of ERC-marker proteins from the pericentrosomal region of the cell.** A) A431 cells were treated with control or Rab11-FIP3 siRNA. Seventy-two hours post-transfection the cells were either processed for immunofluorescence and immunostained with antibodies to RCP, Rab11a, Rab11-FIP4, RME-1 or TfnR, or serum starved before being allowed to internalize Alexa 594-Tfn for 45 min at 37°C before being processed for fluorescence analysis. Scale bar represents 10  $\mu$ m. B) Quantification of the proportion of cells displaying the knockdown phenotype. A minimum of 150 cells per experiment were analysed and the proportion of cells displaying pericentrosomal ERC-marker protein staining was determined. Results are expressed as the mean percentages (from at least three independent experiments)  $\pm$  standard deviation.

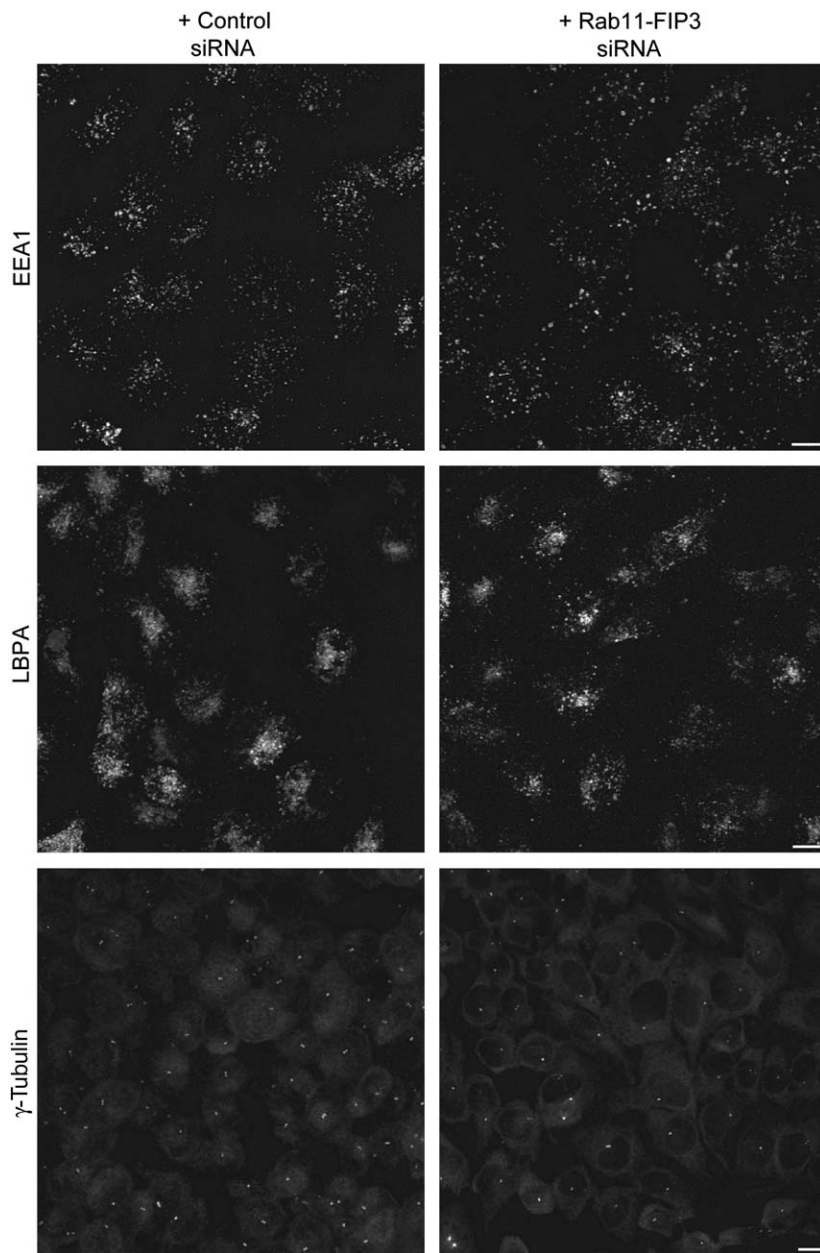


**Figure 3: Sorting endosomes, late endosomes and the centrosome are unaffected by Rab11-FIP3 knockdown.** A431 cells were treated with control or Rab11-FIP3 siRNA. Seventy-two hours post-transfection the cells were processed for immunofluorescence and immunostained with antibodies to EEA1, LBPA or  $\gamma$ -tubulin. These data are typical of at least three separate experiments. Scale bar represents 10  $\mu$ m.

indicates that Rab11 and Nuf are mutually required for their correct intracellular localization (16), we determined if the importance of Rab11-FIP3 for the morphology of the ERC was Rab11 mediated.

To investigate this hypothesis, we examined a mutant of Rab11-FIP3 that is deficient in Rab11 binding. Substitution of the hydrophobic isoleucine residue at position 738 within the Rab-binding domain (RBD) of Rab11-FIP3 to the negatively charged glutamic acid has previously been shown to generate a Rab11-FIP3 mutant that is deficient in Rab11 binding (15). Using dual polarization interferometry (DPI) technology, which allows simultaneous determination of thickness and density of a biological layer on a sensing wavelength surface in real time (26,27), we

investigated the binding affinity of Rab11a Q70L, the GTPase-deficient mutant of Rab11a, for Rab11-FIP3 wild type and Rab11-FIP3 I738E. The kinetic analysis, performed at the early association phase of protein interaction, indicates that the  $K_d$  for the Rab11a Q70L/Rab11-FIP3 wild-type binding was 76 nM, whereas for the Rab11a Q70L-Rab11-FIP3 I738E interaction, a substantially lower affinity of  $K_d = 730$  nM was observed (Figure 5A).

Next, we investigated the intracellular localization of the Rab11-FIP3 I738E mutant and examined the effects its expression has on the morphology of the ERC. We found that in contrast to the wild-type protein, which concentrates in the pericentrosomal region of the cell [Figure S1 (5)], the Rab11-FIP3 I738E mutant localizes predominantly

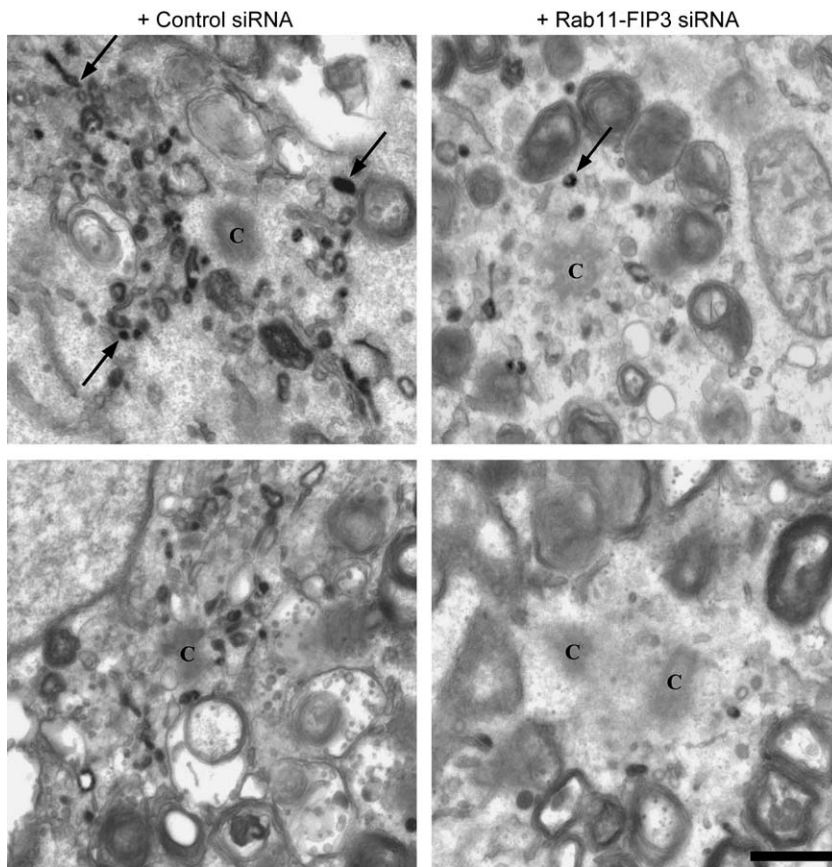


**Figure 4: Tfn-positive vesicles/tubules are absent from the pericentrosomal region of cells devoid of Rab11-FIP3.**

A431 cells were treated with control or Rab11-FIP3 siRNA. Seventy-two hours post-transfection the cells were serum starved before being allowed to internalize Tfn-HRP for 45 min at 37°C, and then processed for electron microscopy analysis. Arrows indicate representative Tfn-HRP-containing structures. 'C' indicates the centrosomes. Scale bar represents 500 nm.

to the cytosol when expressed in A431 cells (Figure 5B). On examination of the localization of ERC-marker proteins in A431 cells expressing Rab11-FIP3 I738E, we found a phenotype that mimics the Rab11-FIP3 knockdown phenotype. In all cells with detectable Rab11-FIP3 I738E expression, ERC-marker proteins are completely lost from the pericentrosomal region of the cell (Figures 5B,C and S2). We found that Rab11a is peripherally distributed on expression of Rab11-FIP3 I738E (Figure 5B). Even in cells expressing almost undetectable levels of Rab11-FIP3 I738E (denoted by asterisks in the brightness adjusted image in Figure 5B), Rab11a is peripherally localized and completely absent from the pericentrosomal region in 100% of transfected cells (Figure 5B,C). Upon staining Rab11-FIP3 I738E-expressing cells for the TfnR, we found that this protein was also completely lost from the pericentrosomal region (Figure 5B,C). Non-transfected cells display pericentrosomal, in addition to more peripheral, staining for the TfnR, in contrast to the transfected cells that possess only the peripheral TfnR staining, even at relatively low levels of Rab11-FIP3 mutant expression (Figure 5B,C). Furthermore, like Rab11a and the TfnR, we found that RME-1 (Figure 5B,C), RCP and Rab11-FIP4 (Figures S2 and 5C) are completely lost from the pericentrosomal region of Rab11-FIP3 I738E-expressing cells, with RCP concentrated at the leading edges (Figure S2). Immunolabelling of Rab11-FIP3 I738E-expressing cells for

EEA1, LBPA and  $\gamma$ -tubulin indicated that early/sorting endosomes and the centrosome are unaffected by Rab11-FIP3 I738E expression (data not shown). Notably, we did find that in a minor proportion (~15%) of Rab11-FIP3 I738E-expressing cells, staining for the late endosomal marker LBPA, appeared reduced (data not shown).

Our knockdown and mutant expression data indicate that Rab11-FIP3 is crucial for the morphological integrity of the pericentrosomal ERC. To establish if this feature was limited to a class II Rab11-FIP, we transfected A431 cells with RCP I621E, an equivalent RCP mutant previously shown to abolish the ability of RCP to interact with Rab11 (28), and examined the effects its expression has on the morphology of the ERC. Unlike Rab11-FIP3 I738E, expression of RCP I621E had no effect on ERC morphology as Rab11a, TfnR and RME-1 staining were unaffected (Figure 6A,B).

Next, we determined the accessibility of fluorophore-labelled Tfn to the pericentrosomal region of cells expressing either Rab11-FIP3 wild type, Rab11-FIP3 I738E or RCP I621E. We found that following 45 min of continuous uptake of Alexa 594-labelled Tfn, the endocytosed ligand was present on the Rab11-FIP3-positive ERC in Rab11-FIP3 wild-type and RCP I621E-expressing cells, as well as non-transfected cells (Figure 7A,B). However,

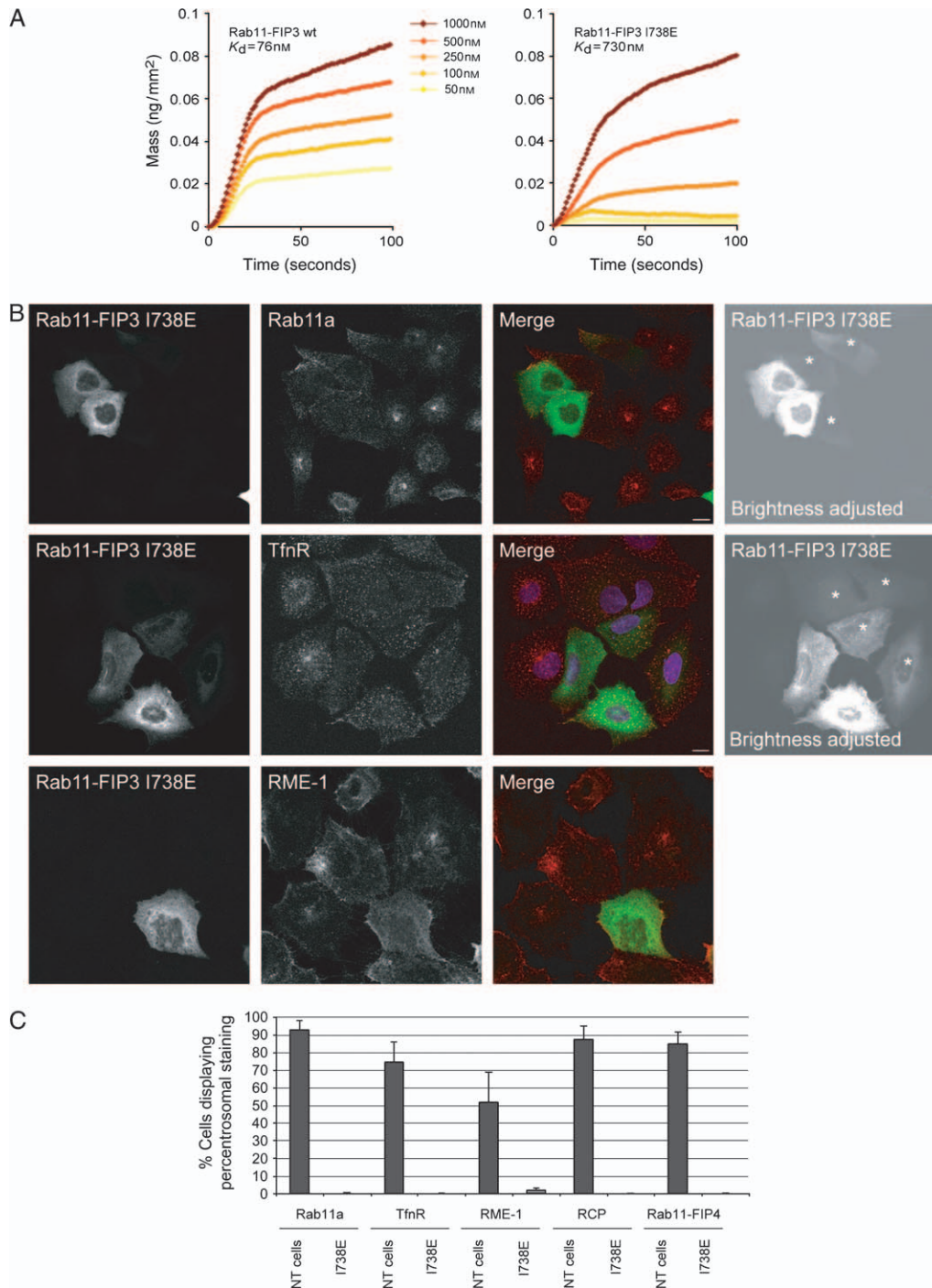


**Figure 5: Rab11-FIP3 ERC function is Rab11 dependent.** A) The Rab11-FIP3 I738E mutant is deficient in Rab11a Q70L binding as determined by DPI. B) A431 cells were transfected with pEGFP-C1/Rab11-FIP3 I738E. Sixteen to eighteen hours post-transfection the cells were processed for immunofluorescence and immunostained with antibodies to Rab11a, TfnR or RME-1. The brightness has been adjusted in the images on the right-hand side to increase the signal visible in cells with very low levels of Rab11-FIP3 I738E expression (asterisks). Scale bar represents 10  $\mu$ m. C) Quantification of the proportion of cells displaying the Rab11-FIP3 I738E phenotype. A minimum of 75 cells per experiment were analysed and the proportion of control [non-transfected (NT)] or Rab11-FIP3 I738E-expressing cells displaying pericentrosomal ERC-marker protein staining was determined. Results are expressed as the mean percentages (from at least three independent experiments)  $\pm$  standard deviation.

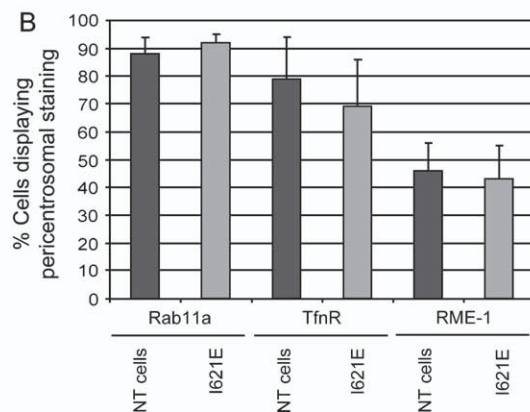
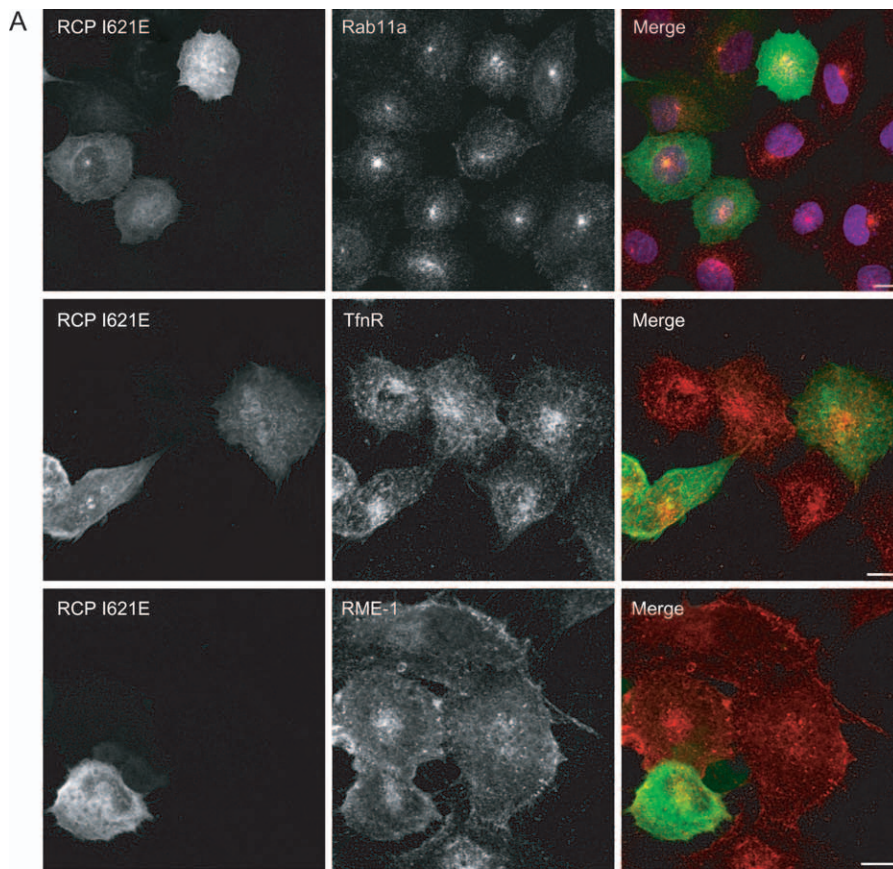


**Figure 6: Rab-coupling protein (RCP) mutant expression does not perturb ERC-marker protein localization.** A) A431 cells were transfected with pEGFP-C3/RCP I621E. Sixteen to eighteen hours post-transfection the cells were processed for immunofluorescence and immunostained with antibodies to Rab11a, TfnR or RME-1. Scale bar represents 10  $\mu$ m. B) Quantification of the proportion of RCP I621E-expressing cells displaying pericentrosomal ERC-marker protein labelling. A minimum of 75 cells per experiment were analysed and the proportion of control [non-transfected (NT)] or RCP I621E-expressing cells displaying pericentrosomal ERC-marker protein staining was determined. Results are expressed as the mean percentages (from at least three independent experiments)  $\pm$  standard deviation.

in Rab11-FIP3 I738E-expressing cells, the Tfn failed to enter the pericentrosomal region of the cell (Figure 7A,B), even in cells expressing low levels of this mutant (Figure 7A, arrow).

Consistent with our Rab11-FIP3 knockdown data, these Rab11-FIP3 I738E expression studies indicate that Rab11-FIP3 is necessary for the structural integrity of the pericentrosomal ERC. This is most likely to be occurring in an Rab11-dependent manner. However, loss of binding to another FIP3 molecule could also lead to the observed results.

#### **Rab11-FIP3 forms extensive coiled-coil domains**

Over the past decade, several large proteins that form extensive coiled-coil structures, and many of which bind Rab GTPases, were found to localize to endosomes and the Golgi [reviewed in Gillingham and Munro (29)]. Most of these proteins play important roles in tethering vesicles to target organelles prior to fusion. Notably, other proteins such as members of the golgin family also play important structural roles as components of a Golgi matrix and as scaffold proteins. Recently, the crystal structure of the carboxy-terminus of Rab11-FIP3 (residues 695–756) in association with Rab11 has been resolved (30,31).

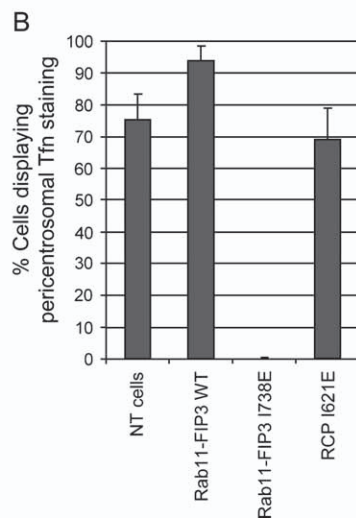
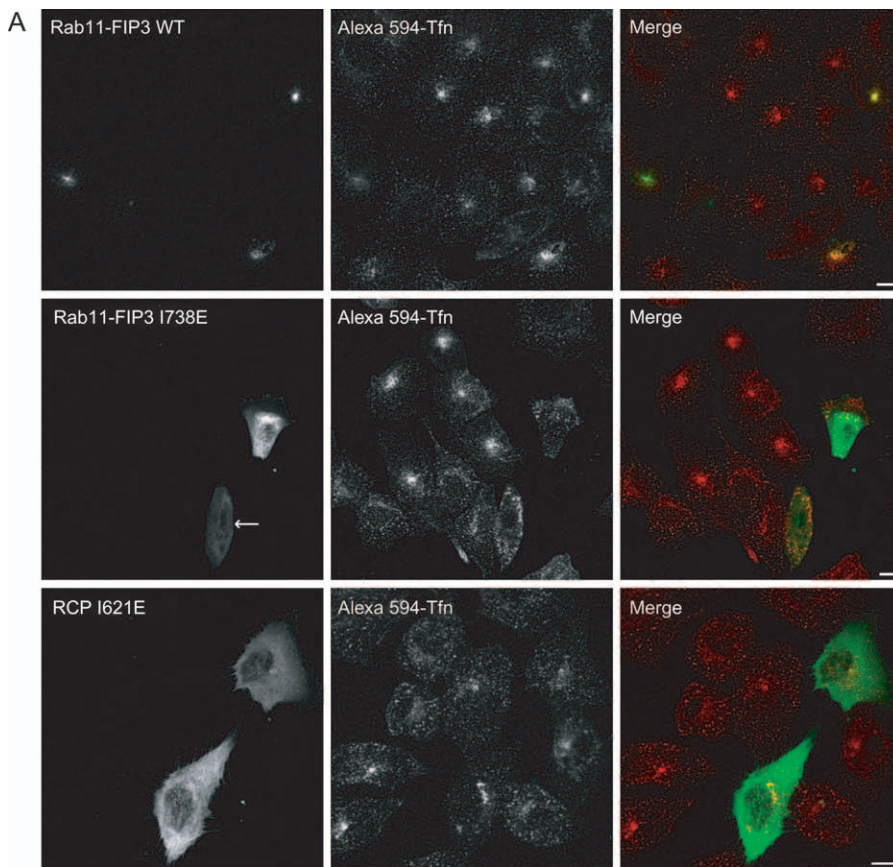


**Figure 7: Tfn is inaccessible to the pericentrosomal region of Rab11-FIP3 I738E-expressing cells.**

A) A431 cells were transfected with pEGFP-C1/Rab11-FIP3 WT, pEGFP-C1/Rab11-FIP3 I738E or pEGFP-C3/RCP I621E. Sixteen to eighteen hours post-transfection the cells were serum starved and then allowed to internalize Alexa 594-Tfn for 45 min at 37°C and processed for fluorescence analysis. The arrow indicates a cell expressing low levels of Rab11-FIP3 I738E. Scale bar represents 10  $\mu$ m. B) Quantification of the proportion of control [non-transfected (NT)] or transfected cells displaying pericentrosomal Alexa 594-Tfn labelling. A minimum of 75 cells per experiment were analysed and results were expressed as the mean percentages (from at least three independent experiments)  $\pm$  standard deviation.

Interestingly, in these studies Rab11-FIP3 and Rab11 crystallized as a heterotetrameric complex [Rab11–Rab11-FIP3(x2)–Rab11] with the RBD of Rab11-FIP3 forming a central  $\alpha$ -helical coiled-coil homodimer. Using the Lupus prediction method, we have previously reported that Rab11-FIP3 is predicted to form coiled-coil structures in a region much longer than that for which the crystal structure is now known (32). Therefore, we investigated if this further region of Rab11-FIP3 indeed assumes a coiled-

coil conformation and determined the importance of this region for its function on the ERC.

To locate possible coiled-coil domains within Rab11-FIP3 with greater accuracy, we applied a combination of additional prediction algorithms to the Rab11-FIP3 sequence. Using the PAIRCOIL algorithm (33), we show that Rab11-FIP3 is predicted to form coiled-coil structures between residues 463 and 692 (Figure S3A). Furthermore, using the

structural disorder prediction algorithm DISOPRED2 (34), we predict a very high level of structural order in the region of Rab11-FIP3 that corresponds to the predicted coiled-coil region (Figure S3A). Interestingly, a break in the predicted coiled-coil domain (around residue 650) detected by the PAIRCOIL program correlates well with a significant increase in predicted disorder in the same region, indicative of a possible discontinuity of the coiled coil (Figure S3A). Additionally, when the Rab11-FIP3 sequence is analysed by the MULTICOIL program (35), which predicts the probability of dimeric and trimeric coiled-coil formation, the highest probability is for the formation of a two-stranded conformation in the Rab11-FIP3 coiled-coil structure (Figure S3B).

As mentioned above, Rab11-FIP3 residues 463–692 were identified as possibly having a coiled-coil structure. Interestingly, this region of Rab11-FIP3 displays strong amino

acid identity with Rab11-FIP4 (Figure S4A), but is not conserved with the class I Rab11-FIPs (Figure S4B). Hexahistidine-fused Rab11-FIP3<sub>(463–692)</sub>, a truncation mutant of the *in silico* predicted coiled-coil region, was analysed by circular dichroism (CD) spectroscopy to test for the presence of a coiled-coil structure. When analysed in the far-UV range, we found that the Rab11-FIP3<sub>(463–692)</sub> fragment displayed a CD spectrum characteristic of proteins with high  $\alpha$ -helical content with negative bands at 222 and 208 nm, and a positive band at 192 nm (Figure 8 A). The ratio of the molar ellipticities at 222 and 208 nm ( $[\theta]_{222}/[\theta]_{208}$ ) has been widely used as an indicator of the microenvironment of helices in proteins, distinguishing between the coiled-coil structure and non-interacting  $\alpha$ -helices (36–40). For a single-stranded  $\alpha$ -helix, the  $[\theta]_{222}/[\theta]_{208}$  ratio ranges from 0.8 to 0.9; conversely, for interacting  $\alpha$ -helices, a higher ratio of  $1.00 \pm 0.03$  is observed (37).

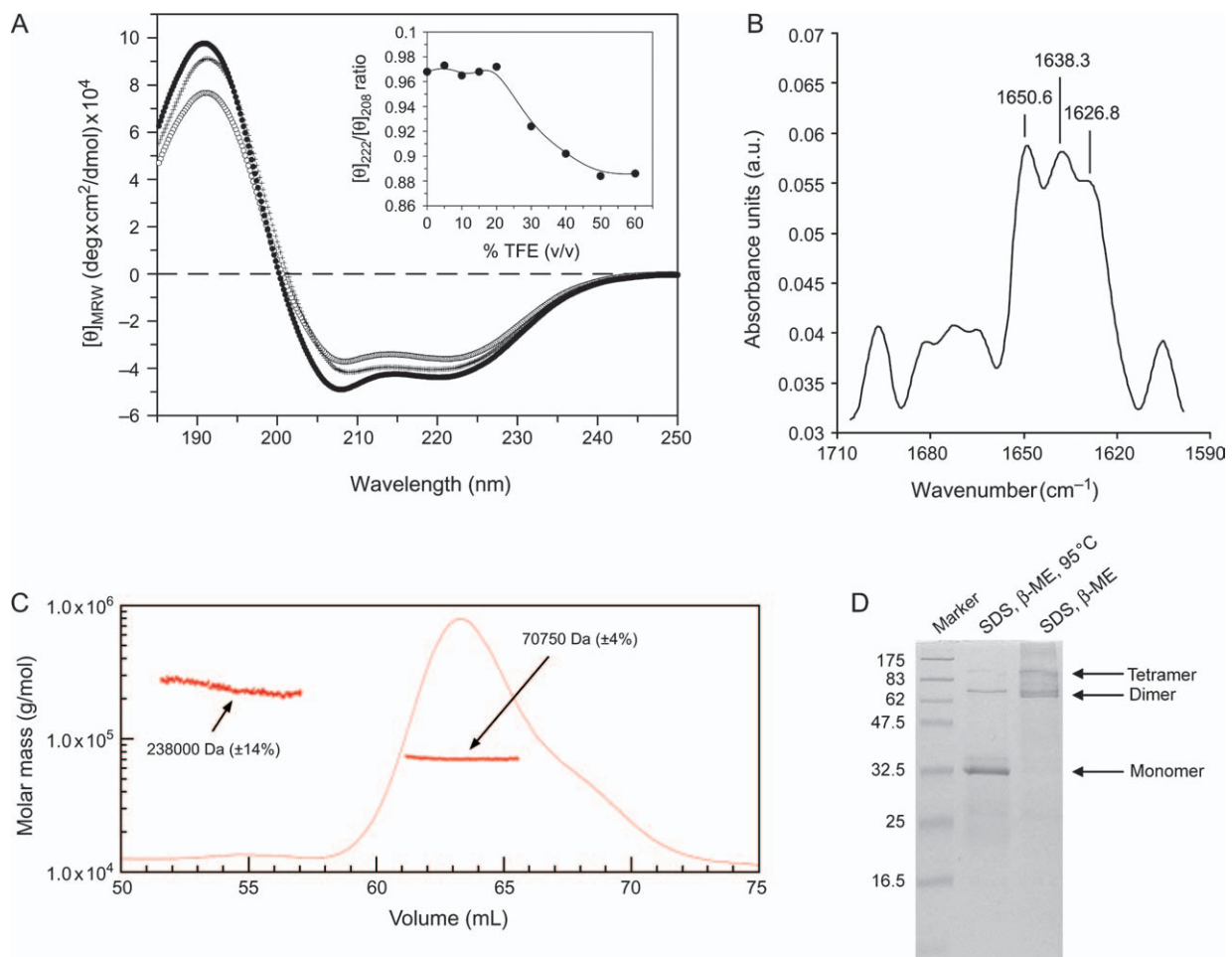


**Figure 8: Rab11-FIP3 forms  $\alpha$ -helical coiled-coil structures.** A) Circular dichroism spectra of the Rab11-FIP3<sub>(463–692)</sub> fragment in 10 mM potassium phosphate (pH 7.3), containing 0% TFE (open circles), 20% (v/v) TFE (crosses) and 50% TFE (filled circles). The inset shows a plot of the ellipticity ratio ( $[\theta]_{222}/[\theta]_{208}$ ) as a function of the TFE concentration. B) Deconvoluted ATR-FTIR spectrum of the Rab11-FIP3<sub>(463–692)</sub> fragment in D<sub>2</sub>O. C) The molecular mass of the Rab11-FIP3<sub>(463–692)</sub> fragment determined by static light scattering. Elution profile of the Rab11-FIP3<sub>(463–692)</sub> (solid line) recorded by the RI detector is presented together with mass calculations for collected peaks (individual data points). D) SDS-PAGE analysis of 5  $\mu$ g of the Rab11-FIP3<sub>(463–692)</sub> fragment. Sample, in denaturing buffer (SDS,  $\beta$ -ME), was prepared with or without heating to 95°C.

In the case of the Rab11-FIP3<sub>(463–692)</sub> fragment, the  $[\theta]_{222}/[\theta]_{208}$  ratio was 0.97, indicating the presence of coiled-coil structures. By densitometry analysis of Western blots, we estimate the cellular concentration of Rab11-FIP3 in A431 cells to be approximately 0.04  $\mu\text{M}$  (data not shown); therefore, the local Rab11-FIP3 concentration on the ERC is likely to be well above 0.1  $\mu\text{M}$ . In addition, we found that the  $[\theta]_{222}/[\theta]_{208}$  ratio is largely unaffected by changing the protein concentration in the range from 5.7 to 0.1  $\mu\text{M}$ , suggesting tight association of  $\alpha$ -helices within a coiled-coil structure of Rab11-FIP3<sub>(463–692)</sub> (data not shown). Together, these data indicate that Rab11-FIP3 is very likely to adopt a coiled-coil conformation *in vivo*.

To confirm the presence of the coiled-coil structure, we examined the Rab11-FIP3<sub>(463–692)</sub> fragment in the presence of increasing concentrations of 2,2,2-trifluoroethanol (TFE). 2,2,2-Trifluoroethanol, commonly used in coiled-coil investigations, stabilizes  $\alpha$ -helical secondary structures, but disrupts tertiary and quaternary structures that are stabilized by hydrophobic forces (37,41,42). It has been previously shown that a 50% TFE concentration is sufficient to disrupt the two-stranded  $\alpha$ -helical coiled coil (37). We found that the Rab11-FIP3<sub>(463–692)</sub> coiled-coil structure appears to be stable at up to 20% TFE (Figure 8A, inset). Above this concentration, the  $[\theta]_{222}/[\theta]_{208}$  ratio begins to drop from the initial value of 0.97 to 0.88 in 50% TFE, but remains unchanged at higher TFE concentrations, indicating that the interacting  $\alpha$ -helices have fully dissociated at 50% TFE (Figure 8A, inset).

In parallel, we performed attenuated total reflection Fourier transform infrared (ATR-FTIR) spectroscopy analysis on the Rab11-FIP3<sub>(463–692)</sub> fragment to further elucidate the structural organization of this polypeptide. In deuterated water ( $\text{D}_2\text{O}$ ), dimeric coiled-coil proteins display ATR-FTIR spectra with at least three separate bands in the amide I region, whereas non-interacting  $\alpha$ -helices display a single band positioned at 1650–1653/cm (43,44). This spectra characteristic is attributed to a distortion of the helical structure by the supercoil bending (43,44). Fourier self-deconvolution of the spectrum of the Rab11-FIP3<sub>(463–692)</sub> fragment in  $\text{D}_2\text{O}$  revealed that the  $\alpha$ -helical amide I band splits into three separate peaks positioned at 1626.8, 1638.3 and 1650.6/cm (Figure 8B). The first and second peaks, having higher area values, are shifted to an atypically low frequency with respect to the standard  $\alpha$ -helical band position (Figure 8B). This unique vibrational spectrum of the Rab11-FIP3 coiled-coil truncation mutant is very similar to the spectrum obtained for tropomyosin, a protein that forms extensive coiled-coil structures (45), and represents the signature of a highly distorted double-stranded  $\alpha$ -helix in parallel orientation (43). These data are in agreement with our MULTICOIL predictions.

Despite the fact that the above results are consistent with the presence of coiled-coil structure within the Rab11-FIP3<sub>(463–692)</sub> fragment, they do not provide definitive

information about its oligomeric state. In order to determine the oligomeric state of the Rab11-FIP3<sub>(463–692)</sub> fragment in solution, we performed multiangle static light scattering (MALS) analysis in chromatography mode. This method provides absolute measurement of molecular weight irrespective of the shape of the protein (46). The calculated molecular weight of hexahistidine-fused Rab11-FIP3<sub>(463–692)</sub> fragment is approximately 33 kDa. However, based on the data derived from the light scattering and refractive index (RI) detectors, the molecular mass of the main peak of this fragment was calculated to be 70 750 Da ( $\pm 4\%$ ), indicating that the Rab11-FIP3<sub>(463–692)</sub> fragment exists as a dimer in solution (Figure 8C). No peak corresponding to the mass of the monomer was detected. The small peak corresponding to  $\sim 238$  kDa ( $\pm 14\%$ ) was attributed to the presence of high-molecular weight proteins, but was considered insignificant because of the very low signal from the RI detector (Figure 8C). In addition to this technique, we found that SDS-PAGE analysis of the Rab11-FIP3<sub>(463–692)</sub> fragment showed that even under denaturing conditions [presence of SDS,  $\beta$ -mercaptoethanol ( $\beta$ -ME), and 95°C heat treatment] a small population of molecules migrate at a molecular weight consistent with a dimer (Figure 8D). Interestingly, the same sample prepared in denaturing conditions (presence of SDS and  $\beta$ -ME), but not heated to 95°C, showed a complete lack of monomers, with the protein migrating predominantly as a dimer, with some tetrameric forms evident (Figure 8D). Notably, based on our bioinformatics analyses, it is probable that this fragment does not adopt a continuous coiled-coil structure, but rather several shorter coiled-coil regions, separated by kinks or short loops induced by the presence of helix-breaking amino acid residues like glycines and prolines. In summary, both the CD and ATR-FTIR data indicate that the Rab11-FIP3<sub>(463–692)</sub> fragment adopts a coiled-coil conformation and our MALS and SDS-PAGE studies indicate that this region of Rab11-FIP3 mediates a dimeric self-interaction.

As outlined previously, Rab11-FIP3 is structurally important for the ERC. Because coiled-coil proteins are often structurally important for organelles (29,47,48), and having determined that Rab11-FIP3 has a coiled-coil structure in the region between residues 463 and 962, we investigated the consequences of expression of a mutant of Rab11-FIP3 that lacks this coiled-coil region. In A431 cells expressing relatively low levels of Rab11-FIP3<sub>( $\Delta$ 463–692)</sub>, a mutant that encodes Rab11-FIP3-lacking amino acids 463–692, the protein concentrated in the pericentrosomal region of the cell where it co-localized with Rab11a (Figure 9, arrow). However, we found that in cells expressing higher levels of Rab11-FIP3<sub>( $\Delta$ 463–692)</sub> the protein was localized to the cytoplasm, the nucleus and in some cells at the cell periphery (Figure 9). Interestingly, in these cells the protein was completely absent from the pericentrosomal region, yet it still co-localized with Rab11a (Figure 9, arrowhead). In addition, we found that other ERC-marker proteins such as RME-1 and endocytosed

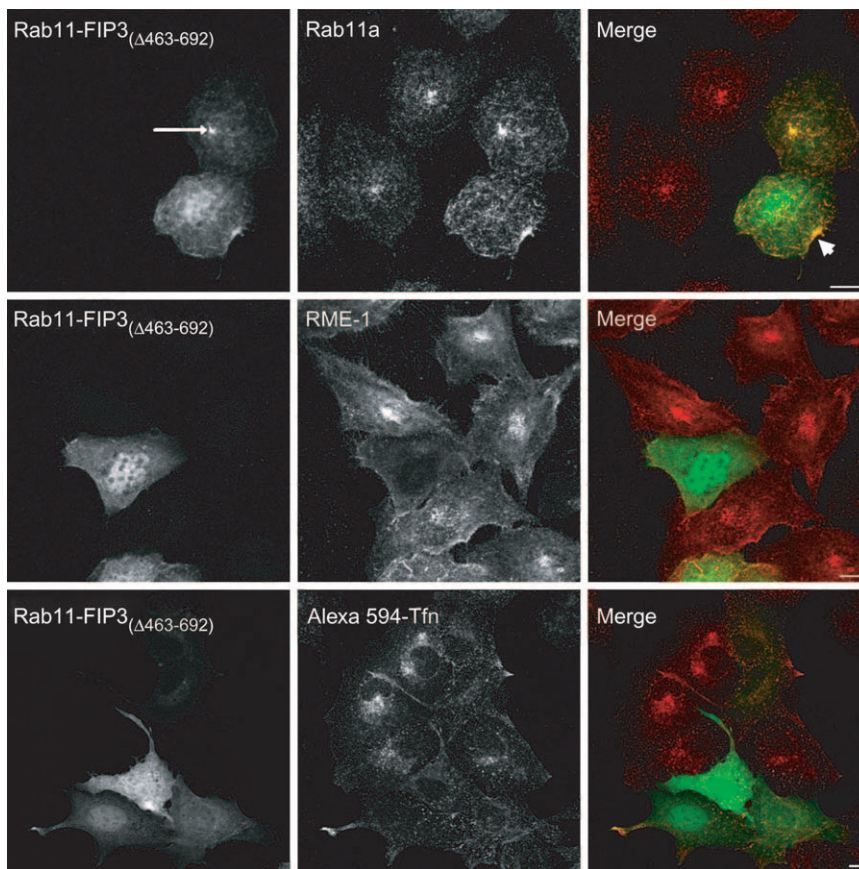


**Figure 9: Deletion of the Rab11-FIP3 coiled-coil region (residues 463–692) disrupts the ERC.** A431 cells were transfected with pEGFP-C1/Rab11-FIP3<sub>(Δ463–692)</sub>. Sixteen to eighteen hours post-transfection the cells were either processed for immunofluorescence and immunostained with antibodies to Rab11a or RME-1, or serum starved and then allowed to internalize Alexa 594-Tfn for 45 min at 37°C before being processed for fluorescence analysis. These data are typical of at least three independent experiments. Scale bar represents 10 μm.

fluorophore-labelled Tfn were also absent from the pericentrosomal region of A431 cells expressing higher levels of Rab11-FIP3<sub>(Δ463–692)</sub> (Figure 9).

Together, these data illustrate that, as predicted, Rab11-FIP3 assumes a coiled-coil structure between residues 463 and 692, and that this region, which is capable of dimerizing, is important to support the function of Rab11-FIP3 on the ERC.

## Discussion

Several reports from various models indicate that the ERC, in a Rab11-dependent fashion, functions in the delivery of membranes to regions of the cell surface that require huge membrane influx for PM reorganization processes such as cell migration, phagocytosis and cytokinesis (5,14,15,49–52). In this context, we and others have identified the Rab11 effector protein, Rab11-FIP3, as a protein of critical importance in the processes of membrane delivery from the ERC to the cleavage furrow during cell division (5,14,15).

To date, the interphase function of Rab11-FIP3 has remained elusive. We noted that the Rab11-FIP3 homologue

in *D. melanogaster*, Nuf, which functions in cellularization and actin remodelling, was recently shown to play a crucial structural role for the ERC (16,17). In *D. melanogaster* SOP cells, which undergo asymmetric division producing two distinct cell types (pIIa and pIIb) that ultimately generate distinct mature sensory organs, only the pIIb cells receive Nuf and can produce a pericentrosomal Rab11-positive ERC (17). As exemplified by our Rab11-FIP3 knockdown data, Rab11-FIP3 has a comparable function to Nuf in mammalian cells. We have found that depletion of Rab11-FIP3 by RNAi results in a loss of all ERC-marker proteins tested, including Rab11a, from their normal pericentrosomal localization. This function for Rab11-FIP3, as a protein of structural importance to the ERC, fits well with our previous findings that overexpression of Rab11-FIP3 alters ERC morphology, condensing it into the pericentrosomal region of the cell.

Rab11-FIP3 function during cell division is proposed to be Rab11 dependent (5,14,15). Additionally, Rab11 and Nuf are mutually required for correct intracellular localization in *D. melanogaster* (16,17). For these reasons, we were prompted to determine if the interphase function of Rab11-FIP3 at the ERC was Rab11 dependent. In this study, we employed the Rab11-binding deficient mutant of Rab11-FIP3, Rab11-FIP3 I738E. We found that expression of the

I738E mutant resulted in loss of the pericentrosomal ERC in a manner that mimics the knockdown phenotype. This effect was observed in 100% of cells expressing the I738E mutant, even at low levels of expression. This indicates that Rab11-FIP3 I738E behaves as a dominant-negative mutant, as its expression adversely affects the normal, wild-type gene product within the same cell. Because we have found that the coiled-coil region of Rab11-FIP3 between residues 463 and 692 dimerizes, it is probable that the I738E mutant interacts with the endogenous protein *in vivo*, thus sequestering it and rendering it non-functional.

In Rab11-FIP3 knockdown samples, only a proportion of cells, albeit substantial, display the loss of the pericentrosomal ERC. This anomaly can be explained by incomplete knockdown of Rab11-FIP3 expression. Indeed, although the transfection efficiency of our siRNA experiments is high, a proportion of Rab11-FIP3 siRNA-treated cells (10–30%, depending on the particular experiment) retain some Rab11-FIP3 staining. Importantly, we have found that the morphological effects we observed on perturbation of Rab11-FIP3 function are not a general Rab11-FIP family feature, as expression of RCP I621E has no such effect. Additionally, we found that the morphological alterations to endosomal structures observed upon interruption of Rab11-FIP3 function are specific to the ERC, as other endosome populations appear largely unaffected.

Coiled-coil domains are ternary structures that consist of two or more  $\alpha$ -helices that twist around one another to form a supercoil. Although coiled-coil proteins have diverse cellular functions, they share a fundamental feature in their ability to hold together molecules, subcellular structures and even tissues [reviewed in Rose and Meier (47)]. It is believed that membrane-bound coiled-coil proteins such as spectrins and golgins serve as structural scaffolds for membranous structures within the cell (29,48,53). Recently, the crystal structure of the carboxy-terminal region of Rab11-FIP3 in complex with Rab11 has been elucidated (30,31). These studies illustrate that Rab11-FIP3 adopts a dimeric coiled-coil structure at its carboxy-terminus in the region encompassing the RBD. However, our data suggest that Rab11-FIP3 is likely to assume a coiled-coil structure over an extensive region (residues 463–692) amino-terminal to this crystallized region. Our findings that Rab11-FIP3 adopts a coiled-coil conformation between residues 463 and 692, and that expression of the Rab11-FIP3 deletion mutant that lacks this coiled-coil region results in loss of the pericentrosomal ERC, fit well with our demonstration that Rab11-FIP3 has a critical structural/tethering role for this organelle. Interestingly, the extensive coiled-coil region in Rab11-FIP3, which has been shown to dimerize, is not conserved within the class I Rab11-FIPs, suggesting that this coiled-coil region is important for an Rab11-FIP3 function that is not shared with the class I Rab11-FIPs. Consistent with this, we have found that expression of an RCP mutant deficient in Rab11 binding does not disrupt the morphology of the peri-

centrosomal ERC. Notably, it remains to be determined if Rab11-FIP4, the second class II Rab11-FIP, serves a similar role to Rab11-FIP3 on the ERC. Our group is currently investigating this question.

In cells expressing low levels of the mutant lacking the coiled-coil region, we do not observe disruption of the ERC. A likely explanation for this is that in cells expressing this mutant, endogenous Rab11-FIP3 is functional until the levels of the mutant protein reaches a critical concentration, whereby it sequesters the endogenous Rab11-FIP3 rendering it non-functional and thus preventing stable maintenance of the ERC. Based on the recent crystallization studies on Rab11-FIP3, this mutant should still self-associate (30,31). Thus, as the deletion mutant lacking the 463–692 coiled-coil region almost certainly has reduced ability to dimerize with endogenous Rab11-FIP3, it may not adversely affect the function of the endogenous protein until higher levels of expression are achieved. Together, these data illustrate that the 463–692 region of Rab11-FIP3 is critical for its function on the ERC, since the ability to associate with Rab11-positive membranes in itself is not sufficient to support its function on this compartment, and suggest that Rab11-FIP3 could form a platform for the recruitment of a protein complex via its coiled-coil region.

Our data, and that in the literature, clearly define functional differences between the two classes of Rab11-FIP proteins. But what specifically is the function of Rab11-FIP3 on the ERC? Does it play a role as a scaffold protein? A scaffold protein, as the name suggests, is a protein whose primary function is to serve as a structural frame, recruiting and connecting other types of proteins. If the scaffold protein, or any protein with which it interacts, can self-interact, one can envisage the formation of a multicomponent protein complex, an event that may be critical for organelle formation and/or stability. The data presented here and previously by our group, coupled with substantial protein–protein interaction data from the literature, are consistent with a role for Rab11-FIP3 as a scaffold protein for the ERC. First, Rab11-FIP3 is known to self-interact (30–32), and to interact with all Rab11 subfamily members (6). Notably, at this point it remains to be determined if the Rab11-FIP3 dimer can simultaneously bind different Rab11 subfamily members. In addition, Rab11-FIP3 possesses a proline-rich amino-terminus, a motif known to mediate a multitude of protein–protein interactions (54). Second, we have established that Rab11-FIP3 adopts an extensive coiled-coil conformation, a common feature among proteins important for organelle structure. Third, overexpression of Rab11-FIP3 profoundly alters the morphology of the Rab11-positive ERC, condensing it into the pericentrosomal region of the cell (5,55). Finally, we have demonstrated that depletion of Rab11-FIP3 by RNAi or perturbation of its function by expression of mutants that are either incapable of binding Rab11 or lack the coiled-coil domain results in loss of the pericentrosomal ERC.

An alternative possibility is that Rab11-FIP3 serves to anchor/tether the ERC to the pericentrosomal region of the cell by binding either directly or indirectly to a minus-end microtubule motor protein, or to a protein that binds specifically to the minus end of microtubules. Indeed, it is well-known that the correct intracellular localization of the ERC requires intact microtubules (56,57), and we have previously found that disruption of the microtubule cytoskeleton with nocodazole causes peripheral distribution of the Rab11-FIP3-positive ERC (5). Investigation of the ability of Rab11-FIP3 to bind microtubules directly or indirectly via an as yet unidentified molecule is an area we now plan to investigate.

In summary, we have defined a specific function for Rab11-FIP3 in formation and/or maintenance of the ERC. Undeniably, the challenge now remains to further dissect the molecular details of how Rab11-FIP3 achieves such a critical function.

## Materials and Methods

### Plasmid construction

pEGFP-C1/Rab11-FIP3, pEGFP-C1/Rab11-FIP3 I738E and pEGFP-C3/RCP I621E have been described elsewhere (5,28,55). pTrcHisC/Rab11-FIP3 and pTrcHisC/Rab11-FIP3 I738E were constructed by subcloning the ~2.4-kb *EcoRI* fragments from the previously described pEGFP-C1/Rab11-FIP3 and pEGFP-C1/Rab11-FIP3 I738E constructs (5,55) into pTrcHisC (Invitrogen, Carlsbad, CA, USA). pEGFP-C2/Rab11-FIP3<sub>(463-692)</sub> was constructed using a sense primer *CC-F* (5'-AAAAGAATTCGCTGACAAGGTTGTCTTCCTG-3') and an antisense primer *CC-R* (5'-AAAGGATCCTGGCTGAGGGTAATGATCTGCC-3') to amplify the cDNA encoding Rab11-FIP3 amino acids 463–692 from pEGFP-C1/Rab11-FIP3. The ~700-bp polymerase chain reaction (PCR) fragment was then cloned into the *EcoRI*–*BamHI* sites of pEGFP-C2 (BD Biosciences, Mountain View, CA, USA). pTrcHisC/Rab11-FIP3<sub>(463-692)</sub> was constructed by subcloning the ~700-bp *BglII*–*BamHI* fragment from pEGFP-C2/Rab11-FIP3<sub>(463-692)</sub> into the *BamHI*–*BglII* sites of pTrcHisC. pEGFP-C1/Rab11-FIP3<sub>(Δ463-692)</sub> was generated by site-directed mutagenesis using the QuickChange Site-Directed Mutagenesis Kit (Stratagene, La Jolla, CA, USA) utilizing a sense primer  $\Delta$ *CC-F* (5'-CCAGAGGAGGACATTATCCAGGCGCCA-3') and an antisense primer  $\Delta$ *CC-R* (5'-TGGCGCCTGGATAATGTCTCTCTGG-3') with pEGFP-C1/Rab11-FIP3 as template. pTrcHisC/Rab11a Q70L was constructed by subcloning the ~850-bp *BamHI*–*PstI* fragment from the previously described pGEM1/Rab11Q70L construct (58) into the *BamHI*–*PstI* sites of pTrcHisC. Constructs generated by PCR were confirmed to be correct by double-strand sequencing.

### Cell lines, plasmid transfection and RNAi

The A431 (epidermal carcinoma) human cell line was cultured in DMEM supplemented with 10% (v/v) foetal bovine serum, 2 mM L-glutamine and 25 mM HEPES and grown in 5% CO<sub>2</sub> at 37°C. For overexpression studies, cells were transfected with plasmid constructs using Effectene (Qiagen, Valencia, CA, USA) as transfection reagent. Rab11-FIP3 expression in A431 cells was depleted by transfection with siGEMONE SMARTpool reagents directed against Rab11-FIP3 (Dharmacon, Chicago, IL, USA). As a control, cells were transfected with siCONTROL non-targeting oligonucleotides (Dharmacon). Control or Rab11-FIP3 siRNA was transfected at a final concentration of 30 nM, using Lipofectamine 2000 according to the manufacturer's instructions (Invitrogen). Seventy-two hours post-transfection the cells were analysed for Rab11-FIP3 expression by immunofluorescence and Western blot.

### Primary antibodies

Mouse monoclonal antibodies to anti- $\gamma$ - and anti- $\alpha$ -tubulin were purchased from Sigma (St. Louis, MO, USA). Mouse monoclonal anti-TfnR and rabbit anti-Rab11a were obtained from Invitrogen. Chicken anti-RCP was from GenWay (San Diego, CA, USA). Mouse monoclonal anti-EEA1 was purchased from Transduction Laboratories (San Jose, CA, USA). Rabbit polyclonal anti-RME-1 antibody was a kind gift from M. S. Robinson. Mouse monoclonal (6C4) anti-LBPA was a kind gift from J. Gruenberg. The rabbit anti-RCP and anti-Rab11-FIP3 antibodies have been described elsewhere (5,7). The anti-Rab11-FIP4 antibody was prepared by immunization of a rabbit with *Escherichia coli*-purified hexahistidine-fused Rab11-FIP4<sub>(82-344)</sub>. The resulting antisera were affinity purified against the immunizing polypeptide.

### Immunoblotting analysis

A431 cells that had been treated with control or Rab11-FIP3 siRNA were resuspended in 50 mM Tris–HCl (pH 7.4), 150 mM NaCl, 1 mM ethylenediaminetetraacetic acid, 0.5% Nonidet P-40 plus protease inhibitors and lysed under rotation for 30 min at 4°C. Cell lysate was then quickly passed six times through a 26-gauge needle. For detection of endogenous proteins, 100  $\mu$ g of total cellular lysate (150  $\mu$ g for Rab11-FIP3 blot) was analysed by SDS–PAGE and immunoblotting.

### Immunofluorescence microscopy

Immunofluorescence microscopy was performed as described previously (55). Secondary antibodies used were goat anti-mouse conjugated to tetramethyl rhodamine isothiocyanate and donkey anti-rabbit conjugated to indocarbocyanine (Cy3), both from Jackson ImmunoResearch (West Grove, PA, USA). Texas Red-conjugated phalloidin was purchased from Invitrogen. For Tfn uptake experiments, cells were serum starved for 1 h and then allowed to internalize Alexa 594-coupled iron-saturated holotransferrin (Invitrogen) at 5  $\mu$ g/mL for 45 min at 37°C before fixation. Coverslips were mounted in Mowiol (Calbiochem, San Diego, CA, USA) and images were recorded using a Zeiss LSM 510 META confocal microscope fitted with a  $\times$  63/1.4 plan apochromat lens. Images were processed using Zeiss LSM Image Browser and ADOBE ILLUSTRATOR software.

### Electron microscopy

A431 cells were cultured on thermanox coverslips (Agar Scientific, Stansted, Essex, UK) and, following incubation with Tfn–HRP for 45 min at 37°C, were incubated post-fixation with 0.0025% hydrogen peroxide and 0.75 mg/mL DAB for 30 min in the dark at room temperature. Coverslips were fixed and processed for electron microscopy as described in (59). Coverslips were mounted on epon stubs, the epon was polymerized overnight at 60°C and the coverslips were removed by heating. Eighty-nanometer sections were cut en face in series and mounted on formvar-coated slot grids. Sections were stained with lead citrate before examination under a JEOL 1010 electron microscope. Images were obtained using a Gatan ORIUS CCD camera.

### Recombinant protein purification

Hexahistidine-fused Rab11-FIP3 wild type and Rab11-FIP3 I738E were purified as previously described for pTrcHisC/Rab11-FIP3 (55). For purification of hexahistidine-fused Rab11-FIP3<sub>(463-692)</sub>, BL21 (DE3) cells were transformed with pTrcHisC/Rab11-FIP3<sub>(463-692)</sub>. A single transformant was grown to an OD<sub>600</sub> = ~0.6 and induced with 0.3 mM isopropylthiogalactoside (IPTG) (Melford, Ipswich, Suffolk, UK) for 12 h at 20°C. For purification of Rab11a Q70L, XL1 cells were transformed with pTrcHisC/Rab11a Q70L. A single transformant was grown to an OD<sub>600</sub> = ~0.6 and induced with 0.4 mM IPTG for 6 h at 27°C. Recombinant proteins were affinity purified using Ni<sup>2+</sup>-NTA agarose beads (Qiagen).

### Dual polarization interferometry

Interactions between hexahistidine-fused Rab11a Q70L and hexahistidine-fused Rab11-FIP3 wild type or Rab11-FIP3 I378E were investigated by the DPI technique using an AnaLight Flex (Farfield Sensors Ltd, Crewe,

Cheshire, UK). The Rab11-FIP3 proteins were immobilized on the surface of unmodified chips on different channels at a concentration of 5  $\mu\text{M}$  in running buffer containing 20 mM HEPES (pH 7.4), 100 mM NaCl and 1 mM  $\text{MgCl}_2$ . Rab11a Q70L was injected at five different concentrations in the same buffer. The  $K_d$  value was calculated from curve fitting over the early association phase from three independent experiments.

### Attenuated total reflection Fourier transform infrared

Attenuated total reflection Fourier transform infrared spectra were recorded on a Bruker Tensor 27 infrared spectrophotometer equipped with a liquid-nitrogen-cooled Mercury Cadmium Tellurium detector in combination with a Bio-ATR II cell. Rab11-FIP3<sub>(463–692)</sub> protein, at a concentration of 2.5 mg/mL, was extensively dialysed at 10°C against buffer prepared with  $\text{D}_2\text{O}$  and containing 100 mM potassium phosphate and 1 mM DTT (pH 7.0). Acquisitions were conducted at 128 scans and a resolution of 4/cm in a volume of 20  $\mu\text{L}$  at 25°C. The spectra were collected from three independent experiments and Lorentzian Fourier self-deconvolution was performed using opus software (Bruker Optics Inc., Ettlingen, Germany).

### CD spectroscopy

Circular dichroism spectra were recorded on an Aviv Model 215 Spectrophotometer (Aviv Biomedical Inc., Lakewood, NJ, USA), equipped with a Peltier temperature controller. Spectra were obtained using either a 10- or a 1-mm quartz Suprasil cuvette (Hellma UK Ltd, Essex, UK) and at a temperature of 23°C, a bandwidth of 1 nm, a stepwidth of 0.2 nm, a response time of 1 second and as an average of five scans. All spectra were baseline corrected, smoothed and converted to mean residue molar ellipticity  $[\theta]_{\text{MRW}}$  ( $\text{deg} \times \text{cm}^2/\text{dmol}$ ). Sample protein concentration was determined by quantitative amino acid analysis (PNAC Facility, Cambridge, UK).

### Multiangle static light scattering

The molar mass ( $M_w$ ) analysis was determined by static light scattering in chromatography mode using a miniDAWN instrument (Wyatt Technology Corp., Santa Barbara, CA, USA) coupled to an AKTA basic fast protein liquid chromatography system (GE Healthcare, Giles, Bucks, UK). A 500- $\mu\text{L}$  aliquot was injected at the flow rate of 0.6 mL/min into the Superdex 200 (10/300) GL column (GE Healthcare) equilibrated in 20 mM Tris, 100 mM NaCl, 1 mM DTT, pH 7.5, buffer. The eluted peaks were passed by RI and MALS detectors. The specific RI increment ( $dn/dc$ ) for each peak was measured and used for calculation of absolute  $M_w$  values using ASTRA software (Wyatt Technology).

### Acknowledgments

The authors are deeply indebted to all members of our laboratory for helpful comments on the manuscript and are especially grateful to Sara Hanscom for her invaluable technical assistance. We are also grateful to Jean Gruenberg for the anti-LBPA antibody and M. S. Robinson for the anti-RME-1 antibody. This work was supported by an Irish Research Council for Science, Engineering and Technology grant (RS/2002/202-6), Science Foundation Ireland (SFI) investigator grants (05/IN.3/B859, 02/IN.1/B032 and 03/IN.3/B371), an SFI equipment supplement grant (02/IN.1/B70S1) and a Wellcome Trust grant (078304).

### Supplementary Materials

**Figure S1: RME-1 co-localizes with Rab11-FIP3 on the ERC.** A431 cells were transfected with pEGFP-C1/Rab11-FIP3 WT. Eighteen hours post-transfection the cells were processed for immunofluorescence and immunostained with an antibody to RME-1. These data are typical of three separate experiments. Scale bar represents 10  $\mu\text{m}$ .

**Figure S2: Rab11-FIP3 I738E expression disrupts the pericentrosomal ERC.** A431 cells were transfected with pEGFP-C1/Rab11-FIP3 I738E. Sixteen to eighteen hours post-transfection the cells were processed for immunofluorescence and immunostained with antibodies to RCP or Rab11-FIP4. These data are typical of four separate experiments. Scale bar represents 10  $\mu\text{m}$ .

**Figure S3: Rab11-FIP3 is predicted to form extensive  $\alpha$ -helical coiled-coil structures.** A) Overlay of plots depicting the probability of forming  $\alpha$ -helical coiled-coil structures in Rab11-FIP3 as determined using PAIRCOIL algorithm (blue) and disorder probability using DISOPRED2 (red). Regions above the dashed line on the DISOPRED2 plot are considered disordered. B) Overlay of plots depicting the probability that Rab11-FIP3 will form a dimeric (blue) or trimeric (green) coiled-coil structure as determined using the MULTICOIL algorithm.

**Figure S4: CLUSTALW alignment of the Rab11-FIPs.** A) CLUSTALW alignment of the class II Rab11-FIPs. Identities are in black and similarities are in grey. Amino acid residues 463–692 of Rab11-FIP3 are underlined in blue. The region of Rab11-FIP3 for which the crystal structure has been solved is underlined in red. B) CLUSTALW alignment of the class I Rab11-FIPs with Rab11-FIP3. Identities are in black and similarities are in grey. Amino acid residues 463–692 of Rab11-FIP3 are underlined in blue.

Supplemental materials are available as part of the online article at <http://www.blackwell-synergy.com>

### References

1. Maxfield FR, McGraw TE. Endocytic recycling. *Nat Rev Mol Cell Biol* 2004;5:121–132.
2. Ullrich O, Reinsch S, Urbe S, Zerial M, Parton RG. Rab11 regulates recycling through the pericentriolar recycling endosome. *J Cell Biol* 1996;135:913–924.
3. Schlierf B, Fey GH, Hauber J, Hocke GM, Rosorius O. Rab11b is essential for recycling of transferrin to the plasma membrane. *Exp Cell Res* 2000;259:257–265.
4. Casanova JE, Wang X, Kumar R, Bhartur SG, Navarre J, Woodrum JE, Altschuler Y, Ray GS, Goldenring JR. Association of Rab25 and Rab11a with the apical recycling system of polarized Madin-Darby canine kidney cells. *Mol Biol Cell* 1999;10:47–61.
5. Horgan CP, Walsh M, Zurawski TH, McCaffrey MW. Rab11-FIP3 localises to a Rab11-positive pericentrosomal compartment during interphase and to the cleavage furrow during cytokinesis. *Biochem Biophys Res Commun* 2004;319:83–94.
6. Hales CM, Griner R, Hobby-Henderson KC, Dorn MC, Hardy D, Kumar R, Navarre J, Chan EK, Lapiere LA, Goldenring JR. Identification and characterization of a family of Rab11-interacting proteins. *J Biol Chem* 2001;276:39067–39075.
7. Lindsay AJ, Hendrick AG, Cantalupo G, Senic-Matuglia F, Goud B, Bucci C, McCaffrey MW. Rab coupling protein (RCP), a novel Rab4 and Rab11 effector protein. *J Biol Chem* 2002;277:12190–12199.
8. Wallace DM, Lindsay AJ, Hendrick AG, McCaffrey MW. Rab11-FIP4 interacts with Rab11 in a GTP-dependent manner and its overexpression condenses the Rab11 positive compartment in HeLa cells. *Biochem Biophys Res Commun* 2002;299:770–779.
9. Lindsay AJ, McCaffrey MW. Rab11-FIP2 functions in transferrin recycling and associates with endosomal membranes via its COOH-terminal domain. *J Biol Chem* 2002;277:27193–27199.
10. Fan GH, Lapiere LA, Goldenring JR, Sai J., Richmond A. Rab11-family interacting protein 2 and myosin Vb are required for CXCR2

- recycling and receptor-mediated chemotaxis. *Mol Biol Cell* 2004;15:2456–2469.
11. Prekeris R, Klumperman J, Scheller RH. A Rab11/Rip11 protein complex regulates apical membrane trafficking via recycling endosomes. *Mol Cell* 2000;6:1437–1448.
  12. Hickson GR, Matheson J, Riggs B, Maier VH, Fielding AB, Prekeris R, Sullivan W, Barr FA, Gould GW. Arfophilins are dual Arf/Rab 11 binding proteins that regulate recycling endosome distribution and are related to *Drosophila* nuclear fallout. *Mol Biol Cell* 2003;14:2908–2920.
  13. Shin OH, Couvillon AD, Exton JH. Arfophilin is a common target of both class II and class III ADP-ribosylation factors. *Biochemistry* 2001;40:10846–10852.
  14. Wilson GM, Fielding AB, Simon GC, Yu X, Andrews PD, Hames RS, Frey AM, Peden AA, Gould GW, Prekeris R. The FIP3-Rab11 protein complex regulates recycling endosome targeting to the cleavage furrow during late cytokinesis. *Mol Biol Cell* 2005;16:849–860.
  15. Fielding AB, Schonteich E, Matheson J, Wilson G, Yu X, Hickson GR, Srivastava S, Baldwin SA, Prekeris R, Gould GW. Rab11-FIP3 and FIP4 interact with Arf6 and the exocyst to control membrane traffic in cytokinesis. *EMBO J* 2005;24:3389–3399.
  16. Riggs B, Rothwell W, Mische S, Hickson GR, Matheson J, Hays TS, Gould GW, Sullivan W. Actin cytoskeleton remodeling during early *Drosophila* furrow formation requires recycling endosomal components nuclear-fallout and Rab11. *J Cell Biol* 2003;163:143–154.
  17. Emery G, Hutterer A, Berdnik D, Mayer B, Wirtz-Peitz F, Gaitan MG, Knoblich JA. Asymmetric Rab 11 endosomes regulate delta recycling and specify cell fate in the *Drosophila* nervous system. *Cell* 2005;122:763–773.
  18. van Ijzendoorn SC. Recycling endosomes. *J Cell Sci* 2006;119:1679–1681.
  19. Zerial M, McBride H. Rab proteins as membrane organizers. *Nat Rev Mol Cell Biol* 2001;2:107–117.
  20. Lin SX, Grant B, Hirsh D, Maxfield FR. Rme-1 regulates the distribution and function of the endocytic recycling compartment in mammalian cells. *Nat Cell Biol* 2001;3:567–572.
  21. Grant B, Zhang Y, Paupard MC, Lin SX, Hall DH, Hirsh D. Evidence that RME-1, a conserved *C. elegans* EH-domain protein, functions in endocytic recycling. *Nat Cell Biol* 2001;3:573–579.
  22. Mu FT, Callaghan JM, Steele-Mortimer O, Stenmark H, Parton RG, Campbell PL, McCluskey J, Yeo JP, Tock EP, Toh BH. EEA1, an early endosome-associated protein. EEA1 is a conserved alpha-helical peripheral membrane protein flanked by cysteine “fingers” and contains a calmodulin-binding IQ motif. *J Biol Chem* 1995;270:13503–13511.
  23. Schmid SL, Cullis PR. Membrane sorting. Endosome marker is fat not fiction. *Nature* 1998;392:135–136.
  24. Oakley BR. Gamma-tubulin: the microtubule organizer? *Trends Cell Biol* 1992;2:1–5.
  25. Peden AA, Schonteich E, Chun J, Junutula JR, Scheller RH, Prekeris R. The RCP-Rab11 complex regulates endocytic protein sorting. *Mol Biol Cell* 2004;15:3530–3541.
  26. Swann MJ, Peel LL, Carrington S, Freeman NJ. Dual-polarization interferometry: an analytical technique to measure changes in protein structure in real time, to determine the stoichiometry of binding events, and to differentiate between specific and nonspecific interactions. *Anal Biochem* 2004;329:190–198.
  27. Cross GH, Reeves AA, Brand S, Popplewell JF, Peel LL, Swann MJ, Freeman NJ. A new quantitative optical biosensor for protein characterisation. *Biosens Bioelectron* 2003;19:383–390.
  28. Lindsay AJ, McCaffrey MW. Characterisation of the Rab binding properties of Rab coupling protein (RCP) by site-directed mutagenesis. *FEBS Lett* 2004;571:86–92.
  29. Gillingham AK, Munro S. Long coiled-coil proteins and membrane traffic. *Biochim Biophys Acta* 2003;1641:71–85.
  30. Eathiraj S, Mishra A, Prekeris R, Lambright DG. Structural basis for Rab11-mediated recruitment of FIP3 to recycling endosomes. *J Mol Biol* 2006;364:121–135.
  31. Shiba T, Koga H, Shin HW, Kawasaki M, Kato R, Nakayama K, Wakatsuki S. Structural basis for Rab11-dependent membrane recruitment of a family of Rab11-interacting protein 3 (FIP3)/arfophilin-1. *Proc Natl Acad Sci U S A* 2006;103:15416–15421.
  32. Wallace DM, Lindsay AJ, Hendrick AG, McCaffrey MW. The novel Rab11-FIP/Rip/RCP family of proteins displays extensive homo- and hetero-interacting abilities. *Biochem Biophys Res Commun* 2002;292:909–915.
  33. Berger B, Wilson DB, Wolf E, Tonchev T, Milla M, Kim PS. Predicting coiled coils by use of pairwise residue correlations. *Proc Natl Acad Sci U S A* 1995;92:8259–8263.
  34. Ward JJ, Sodhi JS, McGuffin LJ, Buxton BF, Jones DT. Prediction and functional analysis of native disorder in proteins from the three kingdoms of life. *J Mol Biol* 2004;337:635–645.
  35. Wolf E, Kim PS, Berger B. MultiCoil: a program for predicting two- and three-stranded coiled coils. *Protein Sci* 1997;6:1179–1189.
  36. Mehboob S, Luo BH, Patel BM, Fung LW. alpha beta Spectrin coiled coil association at the tetramerization site. *Biochemistry* 2001;40:12457–12464.
  37. Lau SY, Taneja AK, Hodges RS. Synthesis of a model protein of defined secondary and quaternary structure. Effect of chain length on the stabilization and formation of two-stranded alpha-helical coiled-coils. *J Biol Chem* 1984;259:13253–13261.
  38. Zhou NE, Kay CM, Hodges RS. Synthetic model proteins. Positional effects of interchain hydrophobic interactions on stability of two-stranded alpha-helical coiled-coils. *J Biol Chem* 1992;267:2664–2670.
  39. Graddis TJ, Myszkowski DG, Chaiken IM. Controlled formation of model homo- and heterodimer coiled coil polypeptides. *Biochemistry* 1993;32:12664–12671.
  40. Choy N, Raussens V, Narayanaswami V. Inter-molecular coiled-coil formation in human apolipoprotein E C-terminal domain. *J Mol Biol* 2003;334:527–539.
  41. Luo P, Baldwin RL. Mechanism of helix induction by trifluoroethanol: a framework for extrapolating the helix-forming properties of peptides from trifluoroethanol/water mixtures back to water. *Biochemistry* 1997;36:8413–8421.
  42. Maroun RG, Krebs D, El Antri S, Deroussent A, Lescot E, Troalen F, Porumb H, Goldberg ME, Fermandjian S. Self-association and domains of interactions of an amphipathic helix peptide inhibitor of HIV-1 integrase assessed by analytical ultracentrifugation and NMR experiments in trifluoroethanol/H<sub>2</sub>O mixtures. *J Biol Chem* 1999;274:34174–34185.
  43. Heimburg T, Schunemann J, Weber K, Geisler N. FTIR-Spectroscopy of multistranded coiled coil proteins. *Biochemistry* 1999;38:12727–12734.
  44. Heimburg T, Schunemann J, Weber K, Geisler N. Specific recognition of coiled coils by infrared spectroscopy: analysis of the three structural domains of type III intermediate filament proteins. *Biochemistry* 1996;35:1375–1382.
  45. Phillips GN Jr, Fillers JP, Cohen C. Tropomyosin crystal structure and muscle regulation. *J Mol Biol* 1986;192:111–131.
  46. Mogridge J. Using light scattering to determine the stoichiometry of protein complexes. *Methods Mol Biol* 2004;261:113–118.
  47. Rose A, Meier I. Scaffolds, levers, rods and springs: diverse cellular functions of long coiled-coil proteins. *Cell Mol Life Sci* 2004;61:1996–2009.
  48. Barr FA, Short B. Golgins in the structure and dynamics of the Golgi apparatus. *Curr Opin Cell Biol* 2003;15:405–413.
  49. Cox D, Lee DJ, Dale BM, Calafat J, Greenberg S. A Rab11-containing rapidly recycling compartment in macrophages that promotes phagocytosis. *Proc Natl Acad Sci U S A* 2000;97:680–685.
  50. Langevin J, Morgan MJ, Sibarita JB, Aresta S, Murthy M, Schwarz T, Camonis J, Bellaiche Y. *Drosophila* exocyst components Sec5, Sec6,

- and Sec15 regulate DE-cadherin trafficking from recycling endosomes to the plasma membrane. *Dev Cell* 2005;9:355–376.
51. Powelka AM, Sun J, Li J, Gao M, Shaw LM, Sonnenberg A, Hsu VW. Stimulation-dependent recycling of integrin beta1 regulated by ARF6 and Rab11. *Traffic* 2004;5:20–36.
  52. Yoon SO, Shin S, Mercurio AM. Hypoxia stimulates carcinoma invasion by stabilizing microtubules and promoting the Rab11 trafficking of the alpha6beta4 integrin. *Cancer Res* 2005;65:2761–2769.
  53. De Matteis MA, Morrow JS. Spectrin tethers and mesh in the biosynthetic pathway. *J Cell Sci* 2000;113:2331–2343.
  54. Kay BK, Williamson MP, Sudol M. The importance of being proline: the interaction of proline-rich motifs in signaling proteins with their cognate domains. *FASEB J* 2000;14:231–241.
  55. Horgan CP, Zurawski TH, McCaffrey MW. Purification and functional properties of Rab11-FIP3. *Methods Enzymol* 2005;403:499–512.
  56. Lin SX, Gundersen GG, Maxfield FR. Export from pericentriolar endocytic recycling compartment to cell surface depends on stable, detyrosinated (glu) microtubules and kinesin. *Mol Biol Cell* 2002;13:96–109.
  57. Lapierre LA, Dorn MC, Zimmerman CF, Navarre J, Burnette JO, Goldenring JR. Rab11b resides in a vesicular compartment distinct from Rab11a in parietal cells and other epithelial cells. *Exp Cell Res* 2003;290:322–331.
  58. Wilcke M, Johannes L, Galli T, Mayau V, Goud B, Salamero J. Rab11 regulates the compartmentalization of early endosomes required for efficient transport from early endosomes to the trans-golgi network. *J Cell Biol* 2000;151:1207–1220.
  59. Stinchcombe JC, Nomoto H, Cutler DF, Hopkins CR. Anterograde and retrograde traffic between the rough endoplasmic reticulum and the Golgi complex. *J Cell Biol* 1995;131:1387–1401.